

Climate-induced oceanic oxygen fluxes: Implications for the contemporary carbon budget

Laurent Bopp,¹ Corinne Le Quéré, Martin Heimann, and Andrew C. Manning

Max-Planck Institut für Biogeochemie, Jena, Germany

Patrick Monfray

Institut Pierre-Simon Laplace/Laboratoire des Sciences du Climat et de l'Environnement, CE Saclay, Gif sur Yvette, France

Received 30 May 2001; revised 29 January 2002; accepted 29 January 2002; published 24 May 2002.

[1] Atmospheric O₂ concentrations have been used to estimate the ocean and land sinks of fossil fuel CO₂. In previous work, it has been assumed that the oceans have no long-term influence on atmospheric O₂. We address the validity of this assumption using model results and observations. Oceanic O₂ fluxes for the 1860–2100 period are simulated using a coupled climate model in which is nested an ocean biogeochemistry model. Simulated oceanic O₂ fluxes exhibit large interannual (± 40 Tmol yr⁻¹) and decadal (± 13 Tmol yr⁻¹) variability, as well as a net outgassing to the atmosphere caused by climate change (up to 125 Tmol yr⁻¹ by 2100). Roughly one quarter of this outgassing is caused by warming of the ocean surface, and the remainder is caused by ocean stratification. The global oceanic O₂ and heat fluxes are strongly correlated for both the decadal variations and the climate trend. Using the observed heat fluxes and the modeled O₂ flux/heat flux relationship, we infer the contribution of the oceans to atmospheric O₂ and infer a correction to the partitioning of the ocean and land CO₂ sinks. After considering this correction, the ocean and land sinks are 1.8 ± 0.8 Pg C yr⁻¹ and 0.3 ± 0.9 Pg C yr⁻¹, respectively, for the 1980s (a correction of 0.1 from ocean to land) and are 2.3 ± 0.7 Pg C yr⁻¹ and 1.2 ± 0.9 Pg C yr⁻¹, respectively, in the 1990–1996 period (a correction of 0.5 from land to ocean). This correction reconciles the 1990s ocean sink estimated by the Intergovernmental Panel on Climate Change Third Assessment Report with ocean models. **INDEX TERMS:** 1615 Global Change: Biogeochemical processes (4805); 4806 Oceanography: Biological and Chemical: Carbon cycling; 1635 Global Change: Oceans (4203); **KEYWORDS:** ocean, oxygen, outgassing, climate change, carbon

1. Introduction

[2] Only about one half of the CO₂ emitted each year from fossil fuel burning remains in the atmosphere. The other half dissolves in the ocean or is taken up by the land biosphere. The quantification of the partitioning between these ocean and land sinks is possible using the observed changes in atmospheric O₂ and CO₂ concentrations and using an estimate of their stoichiometric ratios for fossil fuel burning, ocean, and land processes [Keeling and Shertz, 1992; Keeling *et al.*, 1996; Battle *et al.*, 2000; Prentice *et al.*, 2001]. The current global mix of fossil fuel burning consumes 1.4 mol of O₂ for every mole of CO₂ it releases [Andres *et al.*, 1999]. Land use changes and terrestrial growth consume (or release) 1.1 moles of O₂ for every mole of CO₂ they release (consume) [Severinghaus, 1995]. The dissolution of atmospheric CO₂ in the oceans is a geochemical consequence of the increase of CO₂ in the atmosphere and has no impact on atmospheric O₂. Comparison of the atmospheric O₂ trend (as detected from changes in the atmospheric O₂/N₂ ratio) and the CO₂ trend was used in the Intergovernmental Panel on Climate Change Third Assessment Report (IPCC-TAR) [Prentice *et al.*, 2001] to provide observationally based budgets of fossil fuel CO₂. This study indicated that the

ocean sink was 1.9 ± 0.6 and 1.7 ± 0.6 Pg C yr⁻¹ in the 1980s and the 1990s, respectively, whereas ocean models give larger values in the 1990s compared to the 1980s [Orr *et al.*, 2001].

[3] There is now increasing evidence that the ocean is warming and will continue to warm in the coming decades [Houghton *et al.*, 2001]. In a recent study, Levitus *et al.* [2000] quantified the variations of the observed heat content of the ocean and found a warming between the mid-1950s and mid-1990s of 0.06°C averaged over the entire ocean and 0.3°C over the upper 300 m. This warming has likely affected the air-sea O₂ flux, because the solubility of O₂ in seawater is strongly dependent on temperature. In this paper, we will refer to this solubility change due to ocean's warming as the thermal effect. As increased temperatures result in decreased O₂ solubility, the warming of the last 50 years has led to a net outgassing of O₂ to the atmosphere. This thermal effect is relatively easily quantifiable and was taken into account in recent budget of the carbon cycle [Prentice *et al.*, 2001]. However, in addition, this warming is also likely to lead to changes in ocean dynamics (stratification, convective mixing, and deepwater formation) [Manabe and Stouffer, 1993; Sarmiento *et al.*, 1998], which would in turn impact biological activity [Bopp *et al.*, 2001]. Both the dynamical effect and the production effect would further lead to changes in dissolved O₂ concentrations in seawater and to air-sea O₂ fluxes variations [Sarmiento *et al.*, 1998].

[4] Keeling *et al.* [2001] have estimated that the total air-sea O₂ fluxes induced by global warming could be ~ 3 – 4 times the thermal effect alone. Their estimation method assumes that the spatial relation in the ocean between temperature and dissolved O₂

¹Also at Institut Pierre-Simon Laplace/Laboratoire des Sciences du Climat et de l'Environnement, CE Saclay, Gif sur Yvette, France.

is representative of the temporal evolution. Several modeling studies have already dealt with the global warming impact on air-sea O₂ flux [Matear *et al.*, 2000; Plattner *et al.*, 2001]. These all show significant O₂ outgassing with climate change and a reduction in dissolved O₂ broadly consistent with observations [Matear *et al.*, 2000; Bindoff and McDougall, 2000; Ono *et al.*, 2001]. However, the predicted ratio between the total air-sea O₂ flux and the thermal effect differs greatly.

[5] In this study, we estimate air-sea O₂ fluxes produced by both natural variability and global warming using a fully coupled atmosphere-ocean general circulation model (AOGCM) including ocean biogeochemistry for the 1860–2100 period. For an evaluation of our model, the natural air-sea O₂ fluxes (climatological, seasonal, interannual, and decadal) are compared to observations. Then, the modeled air-sea O₂ fluxes driven by global warming are analyzed. The mechanisms of these long-term changes are investigated, and we assess the assumptions made by Keeling *et al.* [2001] on the total/thermal air-sea O₂ flux relationship. Finally, the potential impact of these changes on atmospheric O₂ concentrations and on the global carbon budget is discussed. We use the observed variations of the oceanic heat content over the last 50 years [Levitus *et al.*, 2000] and the modeled relationship between the air-sea heat and O₂ fluxes to infer corrections on the O₂-based carbon budget of the last 2 decades.

2. Models

2.1. Climate Model

[6] The climate system was simulated from 1860 to 2100 using a fully coupled AOGCM, including the carbon cycle [Dufresne *et al.*, 2002]. This AOGCM uses the ocean model Océan Parallélisé ICE (OPAICE) [Madec *et al.*, 1997] and the atmospheric model Laboratoire de Météorologie Dynamique, version 5 (LMD5) [Sadourny and Laval, 1984]. The ocean model has roughly 4° resolution in the horizontal, with enhanced latitudinal resolution of up to 1° in the equatorial region. It has 30 vertical levels, 10 of which are in the upper 100 m, and includes an explicit parameterization for vertical mixing [Blanke and Delecluse, 1993]. The OPAICE model also includes a sea-ice model taking into account the relevant thermodynamical processes of snow and ice transformations [Filiberti *et al.*, 1999]. The atmospheric model has a longitudinal resolution of 5.6°; latitudinally, resolution varies with the sine of the latitude. The oceanic and atmospheric components are coupled through the coupler Ocean Atmosphere Soil Interface Software (OASIS) [Terray *et al.*, 1995]. Atmosphere-ocean simulations are made without flux corrections.

[7] This AOGCM was then coupled to a land and ocean carbon cycle model [Friedlingstein *et al.*, 1995; Aumont *et al.*, 1999]. First, a control climate simulation in which CO₂ emissions were set to zero was carried out. Then, for a global warming simulation, CO₂ emissions were prescribed using historical emissions from fossil fuel burning and land use change up to 1990 and using the IPCC SRES98-A2 emissions scenario from 1990 to 2100. Over the historical period, this coupled model reproduces the observed rise in atmospheric CO₂ concentration of 80 ppm and reproduces the observed rise of 0.6°C in the global mean temperature. This coupled model produces an ocean CO₂ sink of 2.1 Pg C yr⁻¹ during the 1980s [Dufresne *et al.*, 2002], in the range of other models [Orr *et al.*, 2001]. A description and validation of the global warming simulation are given by Dufresne *et al.*, [2002].

2.2. Ocean Biogeochemical Model

[8] The ocean biogeochemical model used in this study is a Nutrient Phytoplankton Zooplankton and Detritus (NPZD) type

model. This biogeochemical model has been validated against remote sensing observations both for climatological patterns of surface chlorophyll [Aumont *et al.*, 2002] and for interannual variability (C. Le Quéré *et al.*, Climate-induced variability of oceanic stratification, marine biology, and CO₂, 1979–1997, submitted to *J. Geophys. Res.*, 2001) and has been used in a previous global warming study [Bopp *et al.*, 2001].

[9] The model includes five reservoirs: phosphate, phytoplankton, zooplankton, dissolved organic matter, and particulate organic matter (POC). It explicitly represents plankton dynamics and the penetration of light into the euphotic zone. Phytoplankton growth depends on the local conditions of light, temperature, and vertical eddy diffusion, which acts to homogenize the concentration of phytoplankton cells throughout the entire mixed layer. Phytoplankton growth also depends on the local concentration of phosphate, which is the only limiting nutrient in the model. The model considers one class of zooplankton, feeding on both phytoplankton and POC. POC is assumed to sink at a constant rate of 5 m d⁻¹ in the top 100 m of the water column. Part of the POC reaches 100 m depth and thereby contributes to particulate export production. Subsequently, these particles are exported and remineralized instantaneously at depth according to a power-law function derived from sediment trap fluxes [Suess, 1980].

[10] Our biogeochemical simulation was conducted off line: We used archived oceanic three-dimensional fields (advection, eddy diffusion, temperature, and salinity) and surface fields (winds, sea ice, radiation, and water fluxes) from the AOGCM to force a tracer transport version of the Ocean Parallellise Model (OPA). Advective transport of tracers was computed according to the scheme of Smolarkiewicz and Clark [1986], which is little diffusive. Tracers are diffused along isopycnal surfaces [Lazar *et al.*, 1999] with no horizontal background diffusivity. Isopycnal diffusion coefficients are constant at 2000 cm² s⁻¹ everywhere, and vertical diffusion coefficients are computed prognostically using a 1.5 turbulent closure scheme [Blanke and Delecluse, 1993].

[11] Oxygen concentrations are governed in the ocean interior by

$$\frac{\partial O_2}{\partial t} = -\mathbf{u} \cdot \nabla O_2 + \nabla \cdot (\kappa \nabla O_2) + J_{\text{bio}} + J_{\text{flux}}, \quad (1)$$

where $-\mathbf{u} \cdot \nabla O_2$ represents advection with \mathbf{u} as the velocity vector, $\nabla \cdot (\kappa \nabla O_2)$ represents mixing along isopycnal surfaces and vertical mixing with κ as the diffusion tensor, J_{bio} represents both the source of O₂ due to formation of organic matter in the euphotic zone and the loss of O₂ from remineralization, and J_{flux} is the flux of O₂ from air to sea (F_{O_2}) divided by the depth of the surface layer. F_{O_2} is calculated from

$$F_{O_2} = k_w(1 - \gamma_{\text{ice}})(\alpha O_{2\text{atm}} - O_2), \quad (2)$$

where k_w is the transfer velocity and is based on the formulation of Liss and Merlivat [1986]. Air-sea fluxes are reduced by the fraction of ice covering each grid cell (γ_{ice}), and $(\alpha O_{2\text{atm}} - O_2)$ is the difference in O₂ partial pressure between the air and surface sea water. The solubility of O₂ in seawater (α) is computed using the formulation of Weiss [1970]. A constant atmospheric O₂ concentration $O_{2\text{atm}}$ of 20.946% is assumed [Machta and Hughes, 1970].

[12] Tracers fields were initialized with the final steady state distribution of Aumont *et al.* [2002]. A 2500-year biogeochemical simulation was then done to bring our tracers fields to a quasiequilibrium state. This quasiequilibrium state was then used to initialize the simulation in 1860.

2.3. Atmospheric Transport

[13] We used the atmospheric transport model TM3 [Heimann, 1995] to propagate our modeled oceanic fluxes into the atmosphere. TM3 is driven by meteorological fields derived from

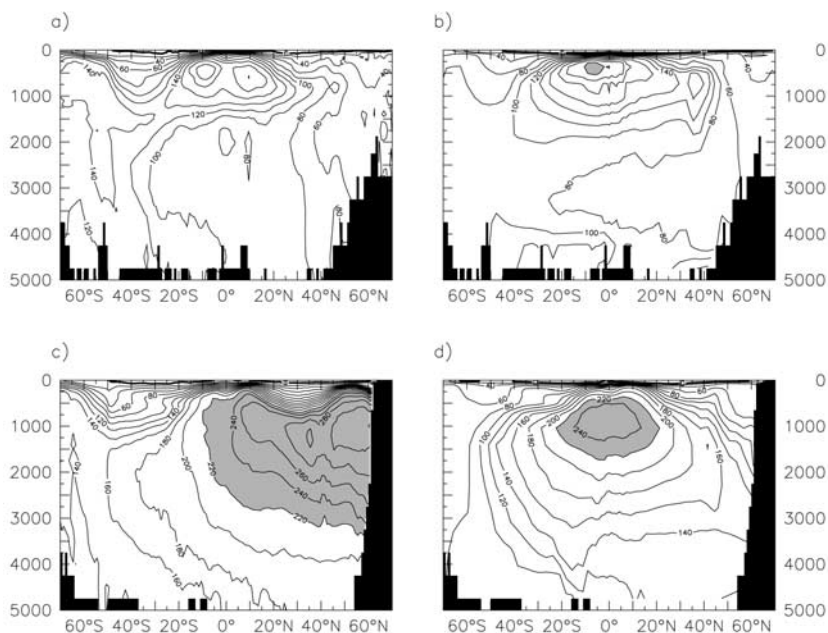


Figure 1. Zonal mean of apparent oxygen utilization (AOU) in $\mu\text{mol L}^{-1}$ for (a, b) Atlantic and (c, d) Pacific. Figures 1a and 1c show observed distributions [Levitus and Boyer, 1994], and Figures 1b and 1d show simulated distributions. Contours are every $20 \mu\text{mol L}^{-1}$.

reanalyses of the European Center for Medium-Range Weather Forecast (ECMWF). The model resolution is 10° longitude by 8° latitude, with 9 vertical levels. An atmospheric simulation of 240 years (from 1860 to 2100) was done in order to compute the evolution of the O_2/N_2 ratio in the atmosphere over that period. However, only one meteorological year (1988) was used here, because we are only interested in the impact of oceanic fluxes alone on the O_2/N_2 ratio in the atmosphere. O_2 and N_2 fluxes (F_{O_2} and F_{N_2}) were transported by the atmospheric model. F_{N_2} was computed off line using the heat fluxes at the air-sea interface with

$$F_{\text{N}_2} = -\frac{Q}{C_p} \frac{\partial \text{N}_2}{\partial T}, \quad (3)$$

where Q is the heat flux of the model and C_p is the heat capacity of seawater. Here we assume that gas exchange coefficients are infinite and thus that N_2 fluxes are in equilibrium, locally, with heat fluxes. F_{O_2} is derived as output of the ocean biogeochemical model.

3. Natural Climate Variability and O₂ Fluxes

[14] We first evaluated the modeled oceanic oxygen cycle by comparing simulated apparent oxygen utilization ($\text{AOU} = \text{O}_2^{\text{sat}} - \text{O}_2$) with observations. AOU is a measure of biologically utilized oxygen and has been used in verifying the accuracy of biological parameterizations in model simulations [Anderson and Sarmiento, 1995]. Our modeled AOU concentrations are broadly consistent with observations from Levitus and Boyer [1994] for both the Atlantic and Pacific basins (Figure 1). The maximum values at middepth are well reproduced by the model. However, some discrepancies remain and seem to be mainly the result of deficiencies in the simulated oceanic circulation. Because of unrealistic deep vertical mixing in the North Pacific, the subsurface maximum in this basin is displaced toward the equator, whereas it is at 50°N in the observations.

[15] Global compilations of air-sea O_2 fluxes are difficult to obtain with the existing observation data sets. Dissolved O_2 in

seawater equilibrates with the atmosphere very quickly (~ 1 month, compared to ~ 1 year for CO_2); thus O_2 fluxes are difficult to estimate. However, it is possible to test our model against seasonal O_2 fluxes [Najjar and Keeling, 2000] and net annual O_2 fluxes [Gruber et al., 2001]. At the interannual and decadal timescale, there are no global data compilations.

[16] To evaluate the modeled natural air-sea O_2 fluxes, we used the first 100 years of the global warming simulation (1860–1960). Air-sea O_2 fluxes were averaged over this period to construct seasonal and annual mean climatologies. Modeled interannual and decadal variability were analyzed over the same period.

3.1. Seasonal Fluxes

[17] On the basis of the ocean oxygen climatology of Najjar and Keeling [1997] and wind speeds from the ECMWF [Gibson et al., 1997], Najjar and Keeling [2000] derived a global monthly mean climatology of air-sea O_2 fluxes. Our modeled fluxes are broadly consistent with the observations, both in phase and in amplitude (Figure 2).

[18] Oxygen is released to the atmosphere during the spring and summer and is taken up by the ocean during the fall and winter. The amplitude of the seasonal cycle is largest between 50° and 60° (north and south), both in the model and in the observations. Poleward of these latitudes the seasonal variations in the flux decrease because of decreases in the gas exchange coefficient.

[19] The seasonal pattern is consistent with thermal, biological, and dynamical forcing. In spring and summer the ocean releases O_2 , first as it warms (solubility pump) and then as phytoplankton blooms develop (biological pump). In fall and winter the ocean takes up O_2 as it cools (solubility pump). At the same time, the ocean also takes up O_2 when the mixed layer deepens and brings deeper waters, depleted in O_2 , in contact with the atmosphere. This last effect is part of the biological pump, because the remineralization of organic matter at depth is responsible for the O_2 depletion of deeper waters.

[20] Simulated seasonal air-sea O_2 fluxes differ, however, from the observations in two main aspects. First, the outgassing in the Southern Ocean starts later in the year in the model, because of a

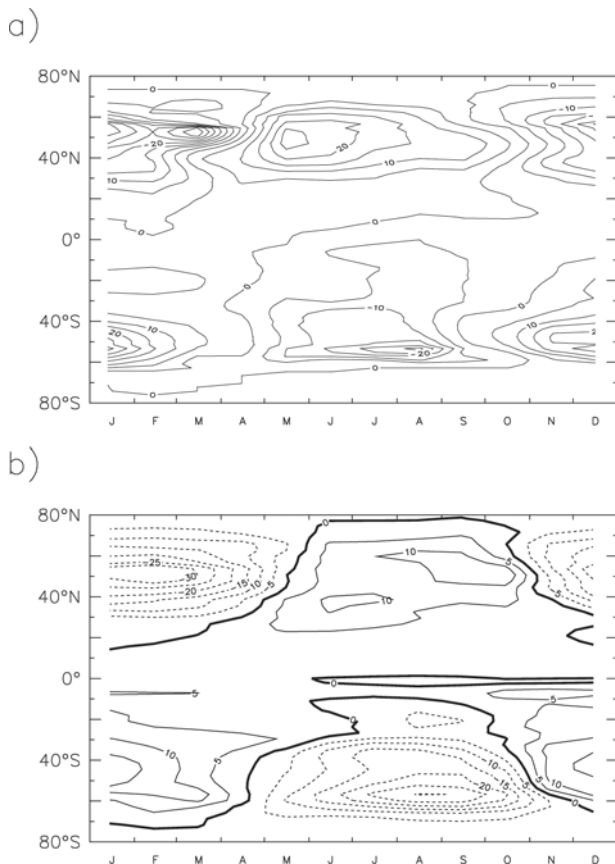


Figure 2. Zonal mean of seasonal cycle of air-sea O₂ flux in mol m⁻² yr⁻¹, (a) based on observations [Najjar and Keeling, 2000] and (b) simulated by the model. Positive values represent outgassing. Contours are every 5 mol m⁻² yr⁻¹.

late shoaling of the mixed layer compared to the observations. Second, the maximum amplitude of O₂ outgassing during the summer is too small in both hemispheres (15 mol m⁻² yr⁻¹, compared to almost 30 mol m⁻² yr⁻¹ in the observations). Nevertheless, our simulated seasonal net outgassing (SNO) of O₂ in each hemisphere (4.3×10^{14} mol yr⁻¹ in the Northern Hemisphere and 8.3×10^{14} mol yr⁻¹ in the Southern Hemisphere) is close to the estimated values proposed by Keeling and Shertz [1992] and Najjar and Keeling [2000] (respectively, 5.5×10^{14} and 7.8×10^{14} mol yr⁻¹ for Keeling and Shertz [1992] and 3.4×10^{14} and 6.1×10^{14} mol yr⁻¹ for Najjar and Keeling [2000]). SNO is defined as the spatially and temporally integrated flux of O₂ when the flux is directed into the atmosphere. The consistent SNO and the weak maximum values of air-sea O₂ fluxes suggest that our simulated biological production is not capturing the peak of the growing season but is consistent with observations when integrated over the entire production season.

[21] We can further test our biogeochemical model by comparing the seasonal variations in atmospheric O₂/N₂ produced by the modeled air-sea O₂ and N₂ fluxes to those observed at several flask sampling stations after correcting for the land contributions (Figure 3). The model reproduces the amplitude of the signal reasonably well, but does not do so well reproducing the phase. A 1- to 2-month lag in the Southern Ocean stations (Cape Grim and Barring Head) is simulated because of the late shoaling of the mixed layer, as already mentioned. Discrepancies are also seen at the La Jolla station and could be due to the selective sampling procedure used at this station [Keeling et al., 1998; Stephens et al.,

1998]. Overall, the comparison is encouraging, with the asymmetric shape reproduced at Cape Grim due to the sharp spring bloom when the mixed layer rapidly stratifies.

3.2. Annual Fluxes

[22] Annual O₂ fluxes are linked to basin-scale transport in the ocean and to biological productivity. Gruber et al. [2001] investigated annual O₂ fluxes for 13 oceanic regions, using an inverse technique independent of air-sea gas exchange parameterizations. They found that the tropical oceans (13°S–13°N) emit large amounts of O₂ (~ 212 Tmol O₂ yr⁻¹), which is compensated by uptake in the Southern Hemisphere (65 Tmol O₂ yr⁻¹) and in the Northern Hemisphere (148 Tmol O₂ yr⁻¹). The predominant pattern that emerges from our simulation is also an uptake of O₂ in the high latitudes of both hemispheres and a release of O₂ in the low latitudes (Figures 4 and 5). The mean annual integrated O₂ flux in the first 100 years of our simulation is close to zero, on average, over the global ocean. The tropical oceans emit 195 Tmol O₂ yr⁻¹, and the Southern (>13°S) and Northern (>13°N) Hemispheres absorb 85 and 119 Tmol O₂ yr⁻¹, respectively. This compares well with Gruber et al. [2001], although our numbers are all somewhat smaller.

[23] This high-latitude/low-latitude pattern is the result of two distinct processes, which reinforce each other. The first process is the change in O₂ solubility driven by cooling of waters at high latitudes and warming of waters at low latitudes. This results in an ingassing of O₂ by the ocean at high latitudes and an outgassing of O₂ at low latitudes (solubility pump). The second process combines dynamical and biological effects and operates generally in the same direction as the solubility pump. At high latitudes, O₂-depleted waters are mixed and transported to the surface from below. This undersaturation in O₂ is not compensated by O₂ biological production (incomplete nutrient utilization), thereby driving an O₂ flux from the atmosphere into the ocean. At low latitudes the O₂ biological production exceeds the oxygen demand created by mixing with undersaturated waters, thereby driving an O₂ flux from the ocean to the atmosphere. However, this overall pattern does not apply in low-latitude upwelling regions (e.g., the equatorial Pacific), where the solubility and biological pumps act in opposite directions. The biological O₂ production does not exceed the oxygen demand created by an intense mixing with undersaturated waters, thereby driving a spatially limited ingassing of O₂ by the ocean that counteracts, locally, the solubility driven outgassing of O₂ (Figure 4).

[24] Our simulated annual O₂ fluxes differ, however, from the data-based estimates of Gruber et al. [2001] in temperate and polar regions (Figure 5). In the Northern Hemisphere our annual ingassing is higher in polar regions and weaker in temperate regions than in the data inversion results. In the Southern Hemisphere, Gruber et al. [2001] estimate that the subpolar South Atlantic is an area of outgassing of O₂, whereas the subpolar regions of the Indian and Pacific Oceans are areas of oceanic uptake of O₂. This pattern could be due to the thermohaline circulation, which drives surface waters to flow northward in the South Atlantic to compensate for the North Atlantic Deep Water formation. Our model does not reproduce this O₂ outgassing in the subpolar South Atlantic.

[25] These discrepancies are mainly the result of deficiencies in the simulated oceanic circulation. The Southern Ocean circulation is particularly sensitive. A better representation of the hydrological cycle in the atmospheric model is needed to properly simulate ocean dynamics in the Southern Ocean. In the ocean, there have been recent improvements in modeling, for example, parameterization of subgrid-scale mixing eddies [Gent et al., 1995] and downslope transport [Beckmann and Döschner, 1997]. Ultimately, though, improving simulations of the Southern Ocean circulation may require much higher resolution and better sea ice models. These discrepancies may also depend on the skill of our model to simulate marine productivity. Limiting nutrients other than PO₄³⁻,

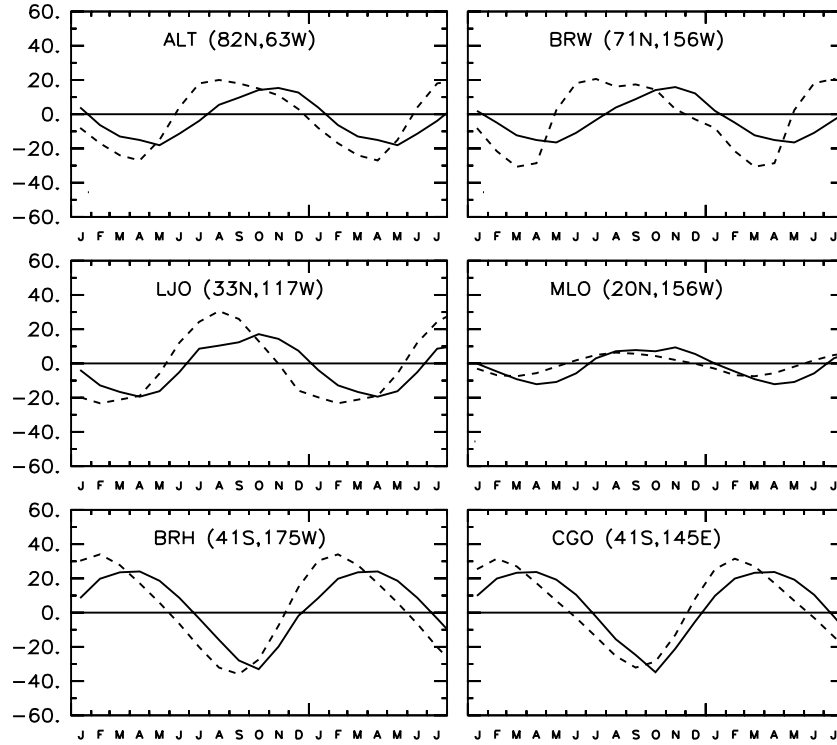


Figure 3. Seasonal variations in atmospheric O₂/N₂ (per meg) after the land contribution has been removed for the six stations of Alert (ALT), Barrow (BRW), La Jolla (LJO), Mauna Loa (MLO), Baring Head (BRH), and Cape Grim (CGO) (dashed lines) and for the model (solid lines). Measurements at Barrow, Cape Grim, and Baring Head are from *Bender et al.* [1996]. Measurements at Alert, La Jolla, and Mauna Loa are from *Stephens et al.* [1998].

such as Fe and Si, are not accounted for in our model. Taking into account these limitations would certainly modify the simulated marine production pattern.

3.3. Interannual to Decadal Fluxes

[26] We used the first 100 years (1860–1960) of the global warming simulation to investigate the interannual (Figure 6a) and decadal (Figure 6b) variations of air-sea O₂ fluxes in the model.

[27] The interannual standard deviation reaches 0.12 mol m⁻² yr⁻¹ (equivalent to 40 Tmol yr⁻¹). The interannual

variability of the flux is dominated by regions of high biological productivity and intense vertical mixing, such as the equatorial Pacific, North Pacific, North Atlantic, and the entire Southern Ocean (Figure 6a).

[28] In the North Atlantic the air-sea O₂ flux exhibits significant interannual variability, with a standard deviation of 0.29 mol m⁻² yr⁻¹ (similar to the model study of *McKinley et al.* [2000]), which is a large fraction of the total mean O₂ ingassing in the basin (1.0 mol m⁻² yr⁻¹). Our simulated variability is linked to the climate variability of our coupled ocean-atmosphere model in the North Atlantic [*Laurent et al.*, 1998].

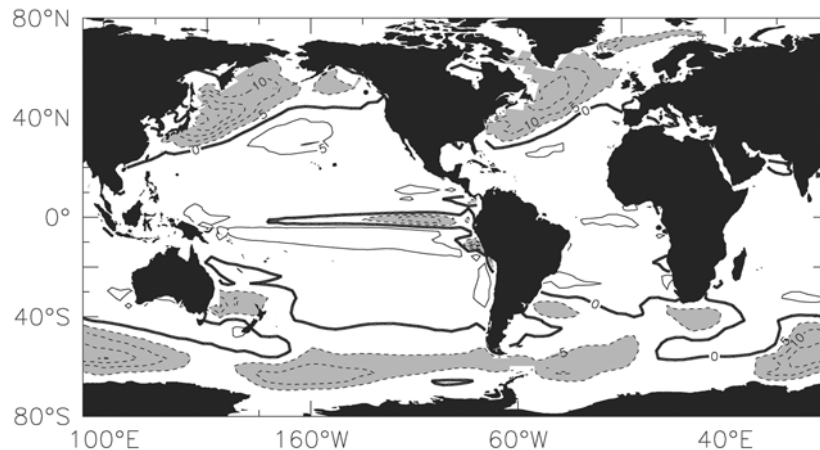


Figure 4. Annual mean O₂ fluxes (mol m⁻² yr⁻¹) for first 100 years of simulation (1860–1960). Positive values represent ocean outgassing. Contours are every 5 mol m⁻² yr⁻¹.

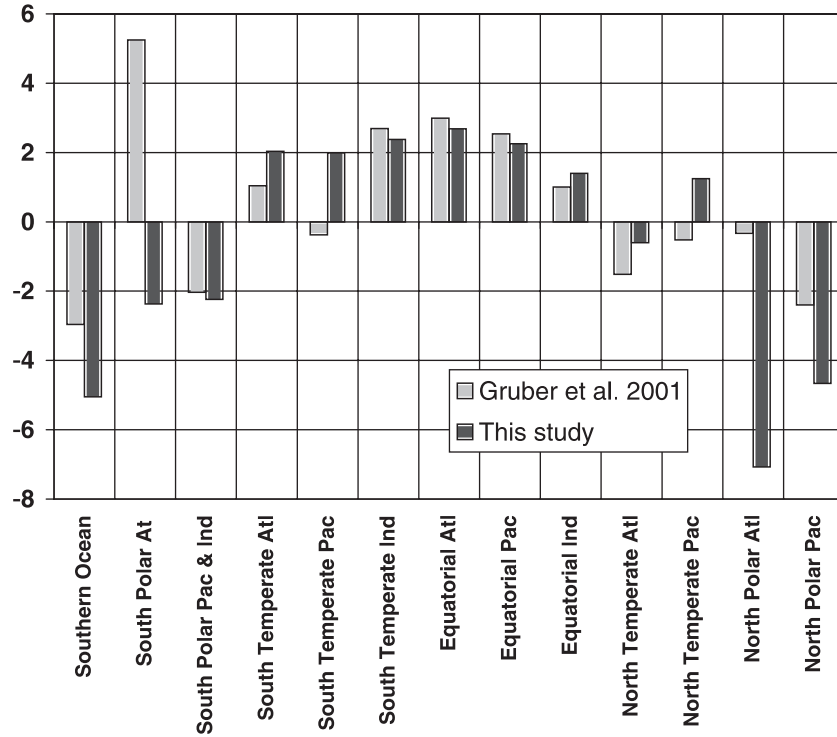


Figure 5. Annual mean O₂ fluxes ($\text{mol m}^{-2} \text{yr}^{-1}$) for first 100 years of simulation (1860–1960) (black) and estimated by the oceanic inversion of Gruber *et al.* [2001] (shaded). Boundaries are at 58°S, 36°S, and 13°S for all basins and at 13°N and 36°N or 58°S for Pacific and Atlantic, respectively.

[29] In the equatorial Pacific we compared modeled interannual variations of surface O₂ concentrations with observations from the National Oceanographic Data Center database. These observations show a peak of the standard deviation of surface O₂ concentrations between 5 and 10 $\mu\text{mol L}^{-1}$ in the east equatorial Pacific, compared to a maximum of 5 $\mu\text{mol L}^{-1}$ in the model. This interannual variability is related to the El Niño–Southern Oscillations. Our model generates El Niño–Southern Oscillations at a frequency of 3–4 years and at an amplitude of about half that observed [Dufresne *et al.*, 2002], which is typical of this kind of coupled model [Tett, 1995; Cox *et al.*, 2000].

[30] In the Southern Ocean, Bender *et al.* [1996] found substantial interannual variability (21% of the mean) in the atmospheric O₂/N₂ ratio measured at two stations where the ocean dominates the atmospheric O₂ signal. Our model also exhibits strong interannual variability in the Southern Ocean (Figure 6a). The O₂ flux interannual variability is primarily a consequence of variability in winter vertical mixing. This variability is induced by simulated Antarctic circumpolar waves [White and Peterson, 1996] that are present in our simulation and already described with the OPA model [Le Quéré *et al.*, 2000].

[31] The decadal standard deviation of the air-sea O₂ flux reaches 0.04 $\text{mol m}^{-2} \text{yr}^{-1}$ globally (equivalent to 13 T mol yr^{-1}) and is dominated by high-latitude regions, with little contributions from low-latitude areas (Figure 6b). The North Pacific exhibits strong decadal variability, but it may not be realistic. Indeed, the only significant long-term drift in the control climate simulation, run in parallel to our global warming simulation, concerns sea ice in the Arctic. Apart from the North Pacific, decadal variability is located mainly around Antarctica (off the Weddell Sea and the Ross Sea and in the Indian sector of the Southern Ocean). This decadal variability is thought to be primarily a consequence of variability in winter time deep con-

vection in these three regions. This may be related to the low-frequency variability in the distribution of sea ice throughout those regions.

4. Climate Change and O₂ Flux

[32] To assess the model performance in predicting air-sea O₂ exchange with global warming, we first compare the simulated increase in ocean heat content with available data.

4.1. Heat Content

[33] In a recent study, Levitus *et al.* [2000] quantified the interannual-to-decadal variability of the heat content of the world ocean for the period 1948–1996, using historical observations. They found a mean warming of 0.3°C for the upper 300 m and 0.06°C for the entire ocean between the mid-1950s and the mid-1990s. The ocean heat content from our coupled model simulation calculated over the same depth ranges is compared to changes in the observed heat content (Figure 7). The trend in the heat content is relatively well reproduced by the model, implying that our climate model is projecting a realistic climate change response. On the basis of a linear trend, the simulated heat content increased by 13×10^{22} J over the 1955–1996 period, which is in relatively good agreement with the observed estimate (18×10^{22} J). The difference between these two numbers may be due to the fact that our coupled model was run without the radiative effects of non-CO₂ greenhouse gases. In addition, substantial differences exist on decadal scales. Our simulated heat content exhibits less variability than the observations, implying that we underpredict decadal variability. Moreover, there are differences in phase. The possible causes of these differences include an underestimation by the model of internal

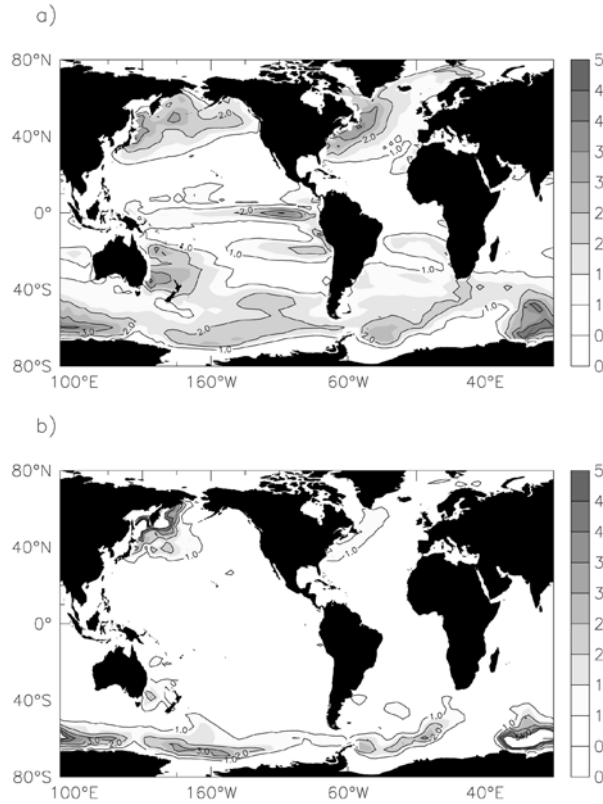


Figure 6. Standard deviation of (a) interannual and (b) decadal variability of O₂ fluxes ($\text{mol m}^{-2} \text{yr}^{-1}$) for first 100 years of simulation (1860–1960). Decadal variability was computed by smoothing at every grid point with a 10-year running average. Interannual variability was computed by removing decadal variability from the total signal. Global mean standard deviations for interannual and decadal variability are 0.12 and $0.04 \text{ mol m}^{-2} \text{yr}^{-1}$, respectively.

variability and the omission of the radiative effects of changes in solar irradiance and volcanic aerosols [Levitus *et al.*, 2001; Barnett *et al.*, 2001].

4.2. O₂ Fluxes and Dissolved O₂

[34] Recently, some studies have shown variations in dissolved O₂ over the last 30–50 years in the Indian Ocean [Bindoff and McDougall, 2000], in the North Pacific [Ono *et al.*, 2001; Emerson *et al.*, 2001], and in the Southern Ocean [Matear *et al.*, 2000]. They all report a significant decrease of O₂ in intermediate waters. The interpretation of this decrease varies from decadal scale change in the carbon export rate to change in ventilation or to slight slowing of the subtropical gyres.

[35] With climate change, our model predicts a decrease in dissolved O₂ broadly consistent with observations and a net outgassing of O₂ from the ocean (Figure 8). In addition to low-frequency variability, our model exhibits a decrease of the global O₂ flux from $-0.10 \text{ mol m}^{-2} \text{yr}^{-1}$ in 1960 to $+0.35 \text{ mol m}^{-2} \text{yr}^{-1}$ in 2100. This outgassing is consistent with the $\sim 0.4 \text{ mol m}^{-2} \text{yr}^{-1}$ outgassing simulated by Matear *et al.* [2000] for 2100. Nevertheless, their predicted outgassing started as early as the first part of the twentieth century, whereas we do not see any climate change impact on air-sea O₂ flux before 1960. Another main difference between these two O₂ simulated fluxes is that our flux exhibits strong interannual-to-decadal variability.

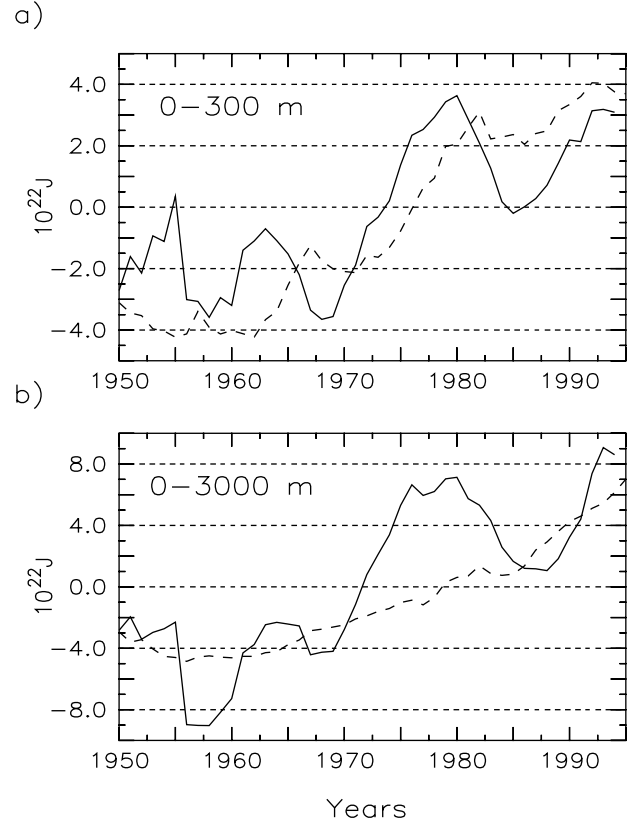


Figure 7. Total heat content of the ocean (10^{22} J) integrated (a) from 0 to 300 m and (b) from 0 to 3000 m for 1950–2000 period. Dashed line is from our model, and solid line is from observations [Levitus *et al.*, 2000].

[36] Differences between 2080–2100 and 1980–2000 show that the major contributors to the outgassing are the Southern Ocean (south of 30°S), the east equatorial Pacific, the North Pacific, and part of the North Atlantic (Figure 9a). Conversely, a few oceanic regions (the west equatorial Pacific and the west Pacific sector of the Southern Ocean) show the opposite tendency (the 2080–2100 to 1980–2000 difference indicates an ingassing of O₂).

[37] The global mean O₂ decrease is $6 \mu\text{mol L}^{-1}$ at the surface, reaches a maximum value of $8 \mu\text{mol L}^{-1}$ in the subsurface ocean

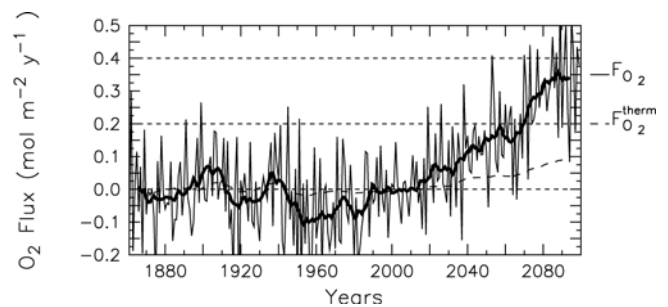


Figure 8. Annual mean O₂ flux (F_{O_2}) simulated over the period from 1860 to 2100. Positive values represent outgassing. Thick solid line is a 10-year running mean that highlights decadal variability and trend. Dashed line is the thermal component ($F_{\text{O}_2}^{\text{therm}}$) of the total O₂ flux. $F_{\text{O}_2}^{\text{therm}}$ is about one quarter of the smoothed F_{O_2} for all of the simulation.

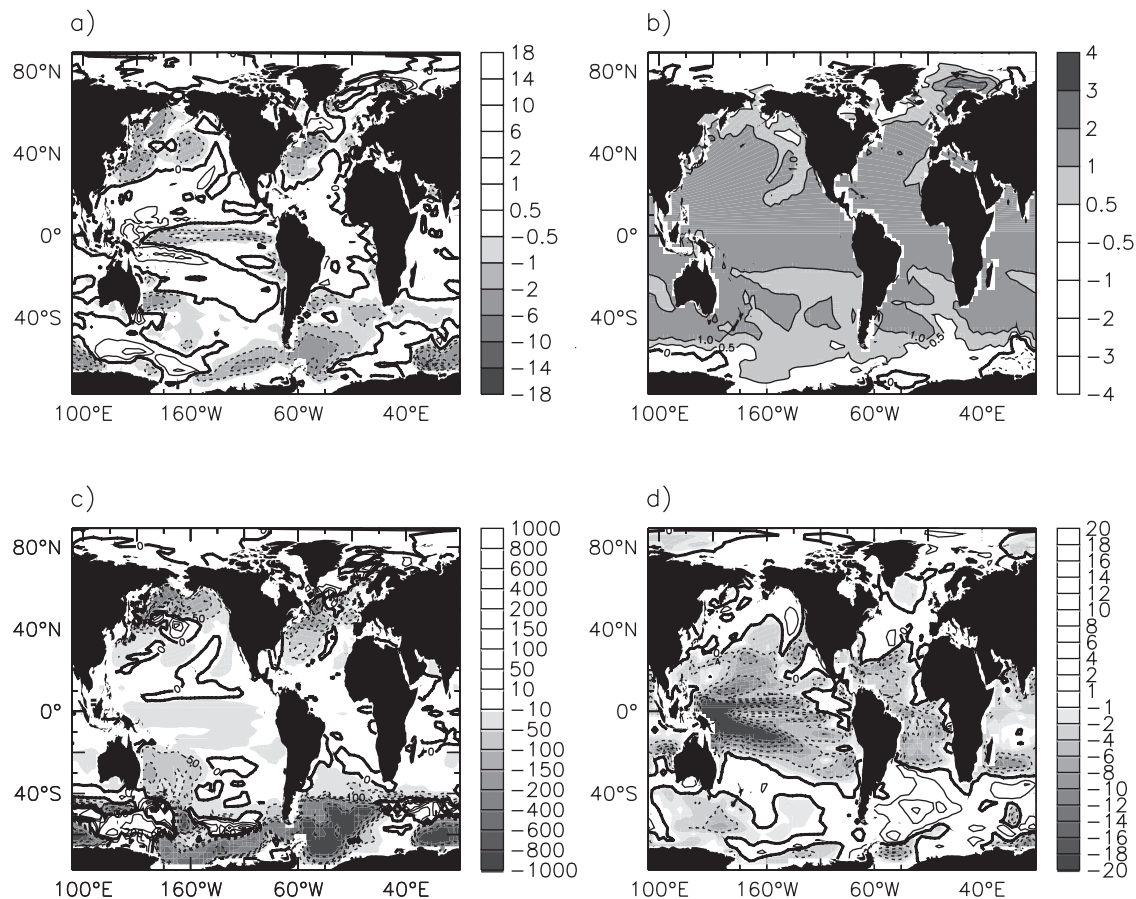


Figure 9. Climate change impact (difference between 2080–2100 and 1980–2000) on (a) O₂ fluxes ($\text{mol m}^{-2} \text{yr}^{-1}$), (b) sea surface temperature (SST) ($^{\circ}\text{C}$), (c) mixed layer depth (m), and (d) export production ($\text{g C m}^{-2} \text{yr}^{-1}$). See color version of this figure at back of this issue.

(100–300 m), and decreases to 3–4 $\mu\text{mol L}^{-1}$ at 3000 m (Figure 10a). The zonal averaged changes in dissolved O₂ show a maximum decrease in O₂ of ~ 15 –20 $\mu\text{mol L}^{-1}$ between 500 and 2500 m at high latitude (Northern and Southern Hemispheres) and

at 200 m in the equatorial region (Figure 10b). Changes in dissolved O₂ are negative everywhere except at the surface south of 60°S. This increase in dissolved O₂ is due to the regional cooling of the surface waters (Figure 9b).

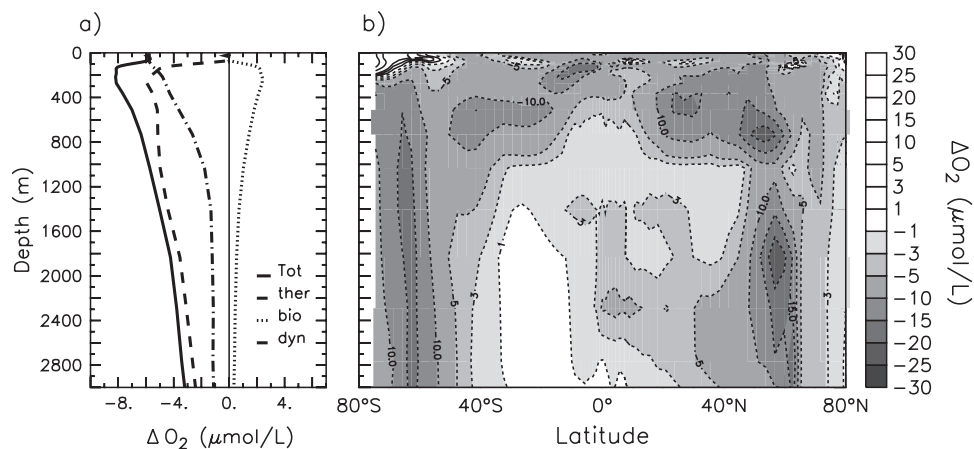


Figure 10. Climate change impact (difference between 2080–2100 and 1980–2000) on (a) vertical profile and (b) zonal mean of dissolved O₂ in the ocean ($\mu\text{mol L}^{-1}$). Contribution of thermal, production, and dynamical effects are also shown in Figure 10a. Thermal effect (blue) is from an additional biogeochemical simulation in which SSTs from the global warming climate run were used as the only impact of global warming on dissolved O₂. Production effect (green) was computed off line using regional changes of export production on O₂ local vertical profile. Dynamical effect (red) was deduced by subtraction from other effects. See color version of this figure at back of this issue.

[38] The vertical pattern of changes in dissolved O₂ (Figure 10a) shows that changes at the surface, which are controlled by changes in O₂ solubility, are smaller than changes at depth or at the subsurface. This implies that the O₂ changes are not only a consequence of the decrease in surface O₂ solubility with warming, but are also driven by changes in the ocean dynamics and/or biology.

4.3. Mechanisms of Outgassing

[39] We now discuss the mechanisms of this outgassing, and we isolate the effects of changes in warming, biology, and ocean dynamics. We can investigate this in more detail by separating the changes in O₂ flux or the changes in dissolved O₂, ΔF_{O_2} and ΔO_2 , respectively, into a thermal effect driven by heat fluxes, a production effect driven by changes in the biological export production, and a dynamical effect driven by changes in the ocean circulation and mixing. The effect of changes in the gas transfer velocity on ΔF_{O_2} was found to be negligible. Thus

$$\Delta F_{O_2} = \Delta F_{O_2}^{\text{therm}} + \Delta F_{O_2}^{\text{prod}} + \Delta F_{O_2}^{\text{dyn}} \quad (4)$$

$$\Delta O_2 = \Delta O_2^{\text{therm}} + \Delta O_2^{\text{prod}} + \Delta O_2^{\text{dyn}}, \quad (5)$$

where the superscripts therm, prod, and dyn denote the thermal, production, and dynamical effects, respectively. These effects represent perturbations of a natural system and thus must be viewed separately from the “biological pump” and “solubility pump” concepts. The thermal effect only impacts the solubility pump, and the production effect only impacts the biological pump. However, changes in ocean dynamics impact both pumps.

[40] Since O₂ air-sea gas exchange is relatively rapid and occurs at a rate similar to heat flux across the air-sea interface, the thermal effect can be estimated from the air-sea heat flux. We computed the thermal effect using the heat flux from the model (Q) and the temperature dependence of the O₂ solubility ($\partial O_2 / \partial T$) from Weiss [1970]. The flux was computed over each grid cell and for every year using the relationship given by equation (6), and then was integrated in space over the whole ocean.

$$F_{O_2}^{\text{therm}} = -\frac{Q}{C_p} \frac{\partial O_2}{\partial T}, \quad (6)$$

where C_p is the heat capacity of sea water. Over the 1860–2100 period the thermal effect represents about one quarter of the total O₂ outgassing (Figure 8). Moreover, the ratio (1/4) between these two fluxes is constant throughout all of the simulated period. This is true for the decadal variations of the first 100 years and for the global warming trend, but not for the interannual variability, which has a stronger biological component.

[41] To investigate how this thermal effect propagates in the ocean’s interior, we performed an additional biogeochemical simulation forced by the output of the control climate experiment, but with sea surface temperatures from the global warming experiment to determine O₂ solubility in seawater. The comparison of the total and thermal effects on the global mean O₂ vertical profile (ΔO_2 and $\Delta O_2^{\text{therm}}$, respectively) confirms, first, that changes in dissolved O₂ at the sea surface are controlled by the thermal effect; second, that the thermal effect is responsible for a 1 $\mu\text{mol L}^{-1}$ decrease in the deep ocean, to be compared to the 4 $\mu\text{mol L}^{-1}$ total decrease; and third, that the thermal effect

decreases the vertical O₂ gradient between the surface and the subsurface, whereas the total ΔO_2 exhibits a stronger gradient with climate change. This stronger gradient may be due to increased export production, ΔO_2^{prod} , and/or to decreased vertical mixing, ΔO_2^{dyn} .

[42] To separate the production and the dynamical effects, we computed off line the impact of changes in export production on dissolved O₂. In the simulation the export production decreases from 11.4 to 10.7 Pg C yr⁻¹ (~6%) between 1980–2000 and 2080–2100 (Figure 9d). To compute the production effect (ΔO_2^{prod}), we assumed that changes in export production would impact the vertical O₂ gradient due to the biological pump. An estimation of the changes in export production and an estimation of the vertical O₂ gradient due to the biological pump would enable us to compute this effect. In the case of a simple two-box model (surface and subsurface), a decrease of 6% of the export production would lead to a decrease of 6% in the O₂ gradient due to the biological pump. To compute this effect, we used (1) the simulated map of changes in export production from 1980–2000 to 2080–2100, (2) the simulated map of the 1980–2000 O₂ vertical gradient, and (3) the simulated map of the 1980–2000 O₂ vertical gradient due to the solubility pump only. From the last two fields we deduced the O₂ vertical gradient due to the biological pump only and applied the changes in export production to this last gradient to estimate, locally, the production effect. The resulting (global mean) ΔO_2^{prod} shows an increase of ~2–3 $\mu\text{mol L}^{-1}$ of dissolved O₂ at a depth of 100–300 m (Figure 10a), which corresponds to a decrease of the mean O₂ vertical gradient, opposite to the total signal.

[43] The last term (ΔO_2^{dyn}) is computed from equation (5). This effect is the major contributor of the decrease in dissolved O₂ in subsurface and deep ocean. This decrease is consistent with a reduction of the convective ventilation of subsurface and deep waters in both hemispheres and with a general decrease in vertical mixing due to the shoaling of the mixed layer depth [Dufresne et al., 2002].

[44] Taking into account these different effects on the O₂ flux, we can explain the different regional patterns found in ΔF_{O_2} (Figure 9a). As discussed above, areas of strong outgassing are found to be areas of strong shoaling of the mixed layer (Figure 9c). In the Southern Ocean and the North Pacific the production effect even reinforces the dynamical effect as the export increases locally (Figure 9d) [Bopp et al., 2001]. In the subtropical gyres of the Pacific and in the entire Atlantic, export production decreases and is responsible for the weak ingassing found between 2080–2100 and 1980–2000.

4.4. Heat Flux/O₂ Flux Relationship

[45] We now discuss the relationship between the total air-sea O₂ flux and the total heat flux across the air-sea interface. Because the total O₂ flux is a multiple of its thermal component over the entire simulation (apart from the interannual variability), we expect to find a strong link between the heat and O₂ fluxes. Figure 11 shows a plot of the total O₂ flux (without interannual variability) versus the total heat flux. The two variables are linearly correlated ($R^2 = 0.95$), with an outgassing of 0.195 mol O₂ m⁻² yr⁻¹, for a warming of 1 W m⁻². As shown for the total O₂ flux/thermal O₂ flux relationship, this slope is the same for the decadal variations of the first 100 years and for the global warming trend. Moreover, this number, equivalent to 6.1 nmol J⁻¹, is very close to the 6 nmol J⁻¹ found by Sarmiento et al. [1998].

[46] To test the robustness of this relationship, two other simulations were used [Friedlingstein et al., 2001; Bopp et al., 2001]. First, using a different climate warming rate (atmospheric pCO₂ increased by 1% yr⁻¹, thus doubling after 70 years) but using the same NPZD biogeochemical model in the ocean, we

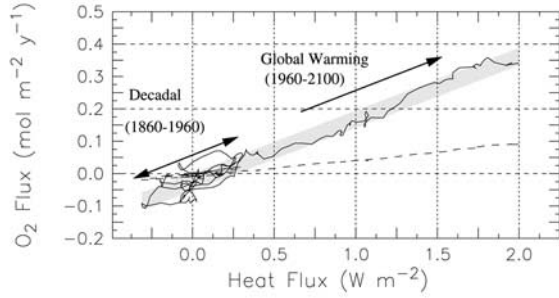


Figure 11. Total heat flux versus total O₂ flux from model (solid line). Interannual variations of total O₂ flux and total heat flux are smoothed with a 10-year running mean. The two variables are linearly correlated ($R^2 = 0.95$), with an outgassing of 0.195 mol O₂ m⁻² yr⁻¹, for a warming of 1 W m⁻². This slope is similar for decadal variations (0.192 for 1860–1960 with $R^2 = 0.56$) and for global warming trend (0.204 for 1960–2100 with $R^2 = 0.97$). Additional curve (dashed line) is total heat flux versus thermal O₂ flux.

found a similar slope of 6.5 nmol J⁻¹ between the total O₂ and the heat fluxes. Second, using this latter climate but using another biogeochemical model (Hambourg Ocean Carbon Cycle model 3 [Maier-Reimer, 1993]), a slope of 6.6 nmol J⁻¹ was found. These sensitivity tests and the comparison to the Sarmiento *et al.* [1998] result suggest that this linear relationship is not very sensitive to the rate of warming or to the model used.

[47] To explain this linear relationship, Keeling *et al.* [2001] proposed to investigate the relationship between O₂^{*} and θ (potential temperature) in the main thermocline. O₂^{*} is a tracer that corrects oxygen concentrations from the influence of biological processes [Gruber *et al.*, 2001].

$$O_2^* = O_2 - r_{O_2:PO_4} PO_4, \quad (7)$$

where $r_{O_2:PO_4}$ is the stoichiometric O₂ to PO₄ ratio in biological processes (photosynthesis and respiration). This ratio is taken to be -172 mol mol⁻¹, from the model parameterization and according to Anderson and Sarmiento [1994]. Variations of O₂^{*} reflect only mixing and the addition or removal of O₂ by air-sea exchange. The same processes (mixing and air-sea fluxes) affect the potential temperature. Available observations [Levitus and Boyer, 1994; Conkright *et al.*, 1994] suggest that O₂^{*} and potential temperature

are strongly negatively correlated (Figure 12a). The model reproduces this strong negative correlation with a similar slope to the one deduced from the observations (Figure 12b). Moreover, this slope does not change significantly with global warming (Figure 12c). Neglecting the effect of changes in biological production on the O₂ flux, Keeling *et al.* [2001] assume that the O₂^{*} - θ slope is equivalent to the ratio between the heat and O₂ fluxes at the air-sea interface. The reason for this assumption is that these O₂^{*} and θ trends in the thermocline drive the ratio between heat and O₂ for the conversion of cold deep waters to warm surface waters and thus for the release of O₂ and the uptake of heat at the air-sea interface. This assumption is valid in our simulation. We have shown that the effect of changes in biological production was relatively small (on the order of 15% of the total effect). Then, we show that the modeled O₂^{*} - θ slope in the thermocline (~ 22 mol L⁻¹ °C⁻¹) is consistent with the modeled ratio between the air-sea heat and O₂ fluxes (~ 6 nmol J⁻¹). Indeed, from this O₂^{*} - θ slope in the thermocline (~ 22 mol L⁻¹ °C⁻¹), divided by the temperature dependence of oxygen saturation (6 mol L⁻¹ °C⁻¹), we can also infer a ratio of $\sim 4/1$, similar to the one found between the total and thermal effects on the air-sea O₂ flux.

5. Implications for the Carbon Budget

[48] We discuss now the implications of this ocean O₂ outgassing for the global carbon budget based on atmospheric O₂ measurements. When used in conjunction with independent estimates of fossil fuel carbon emission and observations of the increase in atmospheric CO₂, observations of the decrease in atmospheric O₂ allow partitioning of the global fossil CO₂ between the ocean and land sinks, as shown graphically by Keeling *et al.* [1996] (Figure 13b). One of the key assumptions made in studies using atmospheric O₂ to constrain this partitioning is that air-sea O₂ fluxes do not contribute to the long-term trend of the atmospheric O₂/N₂ ratio. Therefore a significant net O₂ air-sea flux would result in underestimating or overestimating the oceanic and land carbon sinks.

5.1. Modeled Atmospheric O₂/N₂ Ratios

[49] We first modeled the atmospheric O₂/N₂ ratios over the 1950–2000 period. Air-sea N₂ fluxes were computed from the simulated heat fluxes as described in section 2.3. Air-sea O₂ fluxes were taken from the biogeochemical simulation. Assuming that the 1960–2000 evolution is due only to global warming, we offset the mean O₂ flux value to have a zero mean value over the 1950s.

[50] Over the 1990s decade, oceanic O₂ outgassing resulted in an increase in the atmospheric O₂/N₂ ratio of ~ 7 per meg. For comparison purposes, a change of 4.8 per meg is approximately

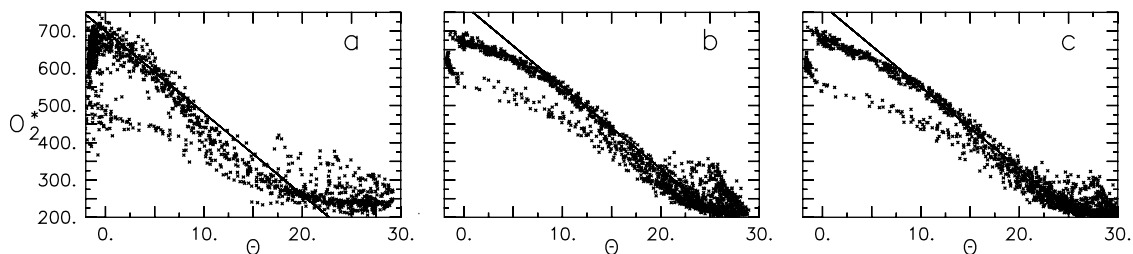


Figure 12. Scatterplot of O₂^{*} (μmol L⁻¹) versus θ (°C) for (a) observations [Levitus and Boyer, 1994; Conkright *et al.*, 1994], (b) model results for 1980–2000, and (c) model results for 2080–2100. Solid line is linear relationship of 22 mol L⁻¹ °C⁻¹ proposed by Keeling *et al.* [2001].

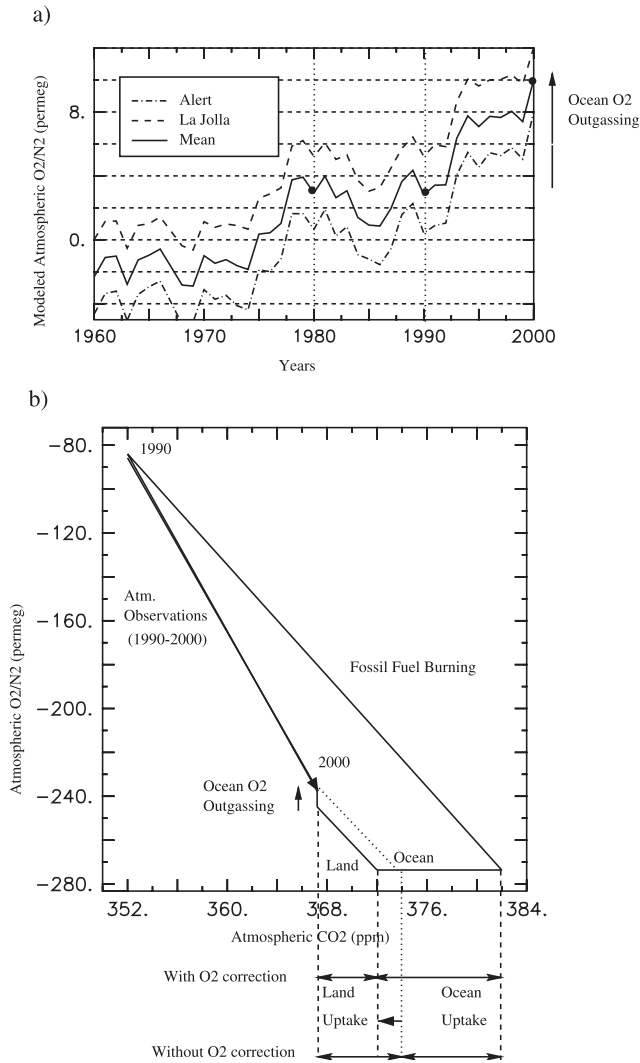


Figure 13. (a) Modeled evolution of O₂/N₂ ratio (permeg) at La Jolla and Alert from 1960 to 2000. (b) Impact of increase in atmospheric O₂/N₂ ratio due to ocean O₂ outgassing on computation of global carbon budget. Dotted line represents CO₂ budget solution without considering impact of ocean O₂ outgassing.

equivalent to a 1-ppm change. This modeled increase is shown for two atmospheric stations (Alert and La Jolla) in Figure 13a. Taking into account this ocean-induced increase in O₂/N₂ ratio leads to a modification of previous estimates of land and ocean CO₂ sinks, as shown graphically in Figure 13b. For the 1990s the 7 permeg increase in O₂/N₂ ratio translates into an underestimation of the ocean sink of $\sim 0.3 \text{ Pg C yr}^{-1}$ and a corresponding overestimation of the land sink of 0.3 Pg C yr^{-1} . Over the 1980s our model does not show any change in the ocean-induced atmospheric O₂/N₂ ratio (Figure 13a).

[51] Our model also provides an error range, which reflects uncertainties around the decadal mean averaged values of the O₂/N₂ ratio. From the decadal standard deviation of the global air-sea O₂ flux, we infer an uncertainty of ± 5 permeg around the decadal mean averaged O₂/N₂ ratio, which leads to an additional $\pm 0.2 \text{ Pg C yr}^{-1}$ uncertainty in the ocean and land sinks. In addition to this calculated uncertainty, we believe that our model underestimates real decadal variability by a factor of 2 (see section 4.1). Doubling the simulated decadal variability

of the air-sea O₂ flux increases the previous value to $\pm 0.4 \text{ Pg C yr}^{-1}$.

5.2. Atmospheric O₂/N₂ Ratios From Observed Oceanic Temperatures

[52] To overcome the fact that the modeled variability is not in phase and may be underestimated when compared to observed decadal variability, we use the heat flux/O₂ flux relationship (Figure 11) from the model and apply it to the data-based oceanic heat flux derived from Levitus *et al.* [2000] (Figure 7b). The heat flux was averaged by decades. Because our relationship between air-sea O₂ and heat fluxes is relevant for both decadal variability and global warming, we used this relationship to infer the mean atmospheric O₂/N₂ ratio variations over the last 50 years. From these variations, we propose the following corrections (Figure 14 and Table 1) for the ocean and land carbon sinks deduced from atmospheric O₂/N₂ ratio measurements.

[53] During the 1980s the ocean heat flux is negative, and computation of carbon sink partitioning without O₂ exchanges with the ocean would overestimate the ocean uptake by 0.1 Pg C yr^{-1} and underestimate the land uptake by the same amount.

[54] During 1990–1996 the ocean heat flux is positive, and the ocean uptake would be underestimated by up to 0.5 Pg C yr^{-1} , with an overestimation by the same amount for the land uptake (Table 1). Ocean heat fluxes are not yet available after 1996. From the standard error on the heat content of Levitus *et al.* [2000] and from the accuracy of our $F_{\text{heat}}/F_{\text{O}_2}$ relationship, we are able to provide an estimate in the uncertainty of the ocean and land sinks. The uncertainty in the mean decadal heat flux computed from Levitus *et al.* [2000] is taken to be $\pm 1 \text{ W m}^{-2}$. The uncertainty in our $F_{\text{heat}}/F_{\text{O}_2}$ relationship is $\pm 0.6 \text{ n mol J}^{-1}$. Thus the resulting uncertainty in the ocean and land sinks is $\pm 0.5 \text{ Pg C yr}^{-1}$.

[55] After considering these corrections, the ocean and land sinks are reevaluated to $1.8 \pm 0.8 \text{ Pg C yr}^{-1}$ and $0.3 \pm 0.9 \text{ Pg C yr}^{-1}$, respectively, for the 1980s and are reevaluated to $2.3 \pm 0.7 \text{ Pg C yr}^{-1}$ and $1.2 \pm 0.9 \text{ Pg C yr}^{-1}$, respectively, for the 1990–1996 period

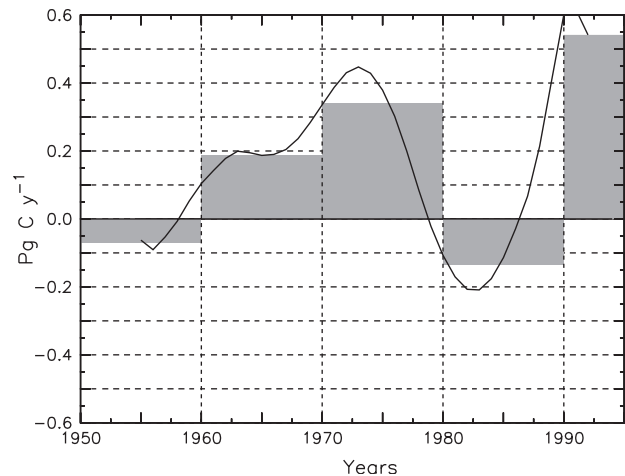


Figure 14. Corrections to estimation of oceanic sink from 1950 to 1996 (Pg C yr^{-1}) if oceanic influence on atmospheric O₂/N₂ ratio is not taken into account for partitioning of carbon sinks. These corrections are based on oceanic heat content estimates of Levitus *et al.* [2000] and on modeled relationship between total heat and total O₂ fluxes. Shown are 10-year running mean (solid line) and 1950s, 1960s, 1970s, 1980s, and 1990–1996 mean values (bars).

Table 1. Global CO₂ Budgets^a

	1980–1989			1990–1996		
	A ^b	B ^c	C ^d	D ^e	B	C
Atmospheric increase	3.3 ± 0.1			2.7 ± 0.1		
Emission (fossil fuel, cement)	5.4 ± 0.3			6.2 ± 0.4		
Ocean-atmosphere flux	−1.9 ± 0.6	+0.1 ± 0.5	−1.8 ± 0.8	−1.8 ± 0.4	−0.5 ± 0.5	−2.3 ± 0.7
Land-atmosphere flux	−0.2 ± 0.7	−0.1 ± 0.5	−0.3 ± 0.9	−1.7 ± 0.7	+0.5 ± 0.5	−1.2 ± 0.9

^a Values given in Pg C yr^{−1}. Boldface denotes differences between the 2 decades. Heat fluxes are not available after 1996.

^b From International Panel on Climate Change (IPCC) 2001 [Prentice et al., 2001]. Thermal effect on O₂/N₂ term is close to 0 for 1980s [Levitus et al., 2000].

^c Correction terms derived from observed heat fluxes [Levitus et al., 2000] and modeled O₂/heat fluxes relationship (section 5.3).

^d Corrected ocean and land sinks using (A + B) for the 1980s and (D + B) for 1990–1996.

^e Identical data and methodology as IPCC 2001 estimate [Prentice et al., 2001], but for 1990–1996. Thermal effect on the O₂/N₂ term, included in the IPCC 2001 computation (0.1 ± 0.1 Pg C yr^{−1}), is not included here because it is already taken into account in (B).

(Table 1). For the oceans, this correction reconciles the carbon uptake estimates based on atmospheric CO₂ and O₂ with estimates from ocean models [Orr et al., 2001]. Indeed, ocean models give a larger ocean sink in the 1990s than in the 1980s (approximately +0.3 Pg C yr^{−1} when forced with observed atmospheric CO₂), whereas the atmospheric O₂ based estimates, when ocean O₂ outgassing is not considered, give a smaller sink during 1990–1996 than in the 1980s (−0.1 Pg C yr^{−1}), but give a larger sink when O₂ outgassing is considered (+0.5 Pg C yr^{−1}).

6. Conclusion

[56] We use a coupled climate-ocean biogeochemistry model to assess the long-term influence of the ocean on atmospheric O₂/N₂ ratios. Our model shows a decrease in oceanic O₂ inventory, due to climate change, that is broadly consistent with observations [Pahlow and Riebesell, 2000; Shaffer et al., 2000; Emerson et al., 2001] and with an oceanic O₂ outgassing consistent with previous model estimates [Sarmiento et al., 1998; Matear et al., 2000; Plattner et al., 2001], but with strong decadal variability. The processes responsible for the O₂ outgassing and for the parallel reduction in dissolved O₂ are (1) changes in surface water solubility due to temperature increase (thermal effect), (2) changes in biological production (production effect), and (3) changes in ocean circulation (dynamical effect). The thermal effect accounts for ~25% of the total outgassing, which is consistent with estimates based on observations [Keeling et al., 2001] and on one other model result [Plattner et al., 2001]. The production effect leads to an ingassing of O₂ due to a decrease in export production. The dynamical effect, through surface stratification and decreased formation of intermediate and deep waters, is the major contributor of the O₂ outgassing by reducing ventilation of O₂-depleted waters.

[57] The climate change—induced outgassing and the decadal variability of the O₂ flux suggest that ocean and land carbon sinks may be overestimated or underestimated by a few tenths of 1 Pg C yr^{−1} in budgets of anthropogenic CO₂ estimated using atmospheric O₂/N₂ ratio trends [Keeling and Shertz, 1992; Bender et al., 1996; Battle et al., 2000; Prentice et al., 2001]. Our model suggests that the global air-sea O₂ flux is strongly correlated to the global air-sea heat flux, as postulated by Keeling et al. [2001]. Using our modeled O₂ flux/heat flux relationship and the ocean heat flux derived from observations [Levitus et al., 2000], we estimate the ocean contribution to atmospheric O₂/N₂ ratio for 1950–1996. Our results suggest that the ocean carbon uptake based on atmospheric O₂/N₂ ratios and estimated without considering ocean O₂ outgassing is overestimated by 0.1 Pg C yr^{−1} in the 1980s and underestimated by 0.5 Pg C yr^{−1} over the 1990–1996 period. Consequently, land carbon uptake is underestimated by 0.1 Pg C yr^{−1} in the 1980s and overestimated by

0.5 Pg C yr^{−1} over the 1990–1996 period. Considering only the thermal effect on O₂ outgassing [Prentice et al., 2001] takes into account only about one quarter of this correction.

[58] For the oceans, this correction reconciles the recent ocean sink estimated by the IPCC-TAR [Prentice et al., 2001] with ocean models. For the land, this correction suggest that the 1990s sink is larger than the 1980s sink by almost 1 Pg C yr^{−1}.

[59] Considering ocean O₂ outgassing is an important step for increasing the precision of CO₂ budget calculations. However, this correction relies on oceanic heat fluxes and on the relation to O₂ fluxes, which has large uncertainties. To reduce these uncertainties, global monitoring of ocean temperature, stratification, and O₂ is required, particularly at the remote high latitudes of the Southern Ocean.

[60] **Acknowledgments.** We thank J.-L. Dufresne, L. Fairhead, and P. Friedlingstein for the climate coupled simulations, O. Aumont for providing the biogeochemical model, and C. Rödenbeck for helping with the TM3 model. We thank S. Levitus, R. Najjar, and N. Gruber for sharing their data sets. We thank R. Keeling and E. Gloor for fruitful discussions. We thank S. Emerson for his review, which greatly improved the paper. The computer time was provided by IDRIS (project 100040).

References

- Anderson, L., and J. Sarmiento, Redfield ratios of remineralization determined by nutrient data analysis, *Global Biogeochem. Cycles*, 8, 65–80, 1994.
- Anderson, L., and J. Sarmiento, Global ocean phosphate and oxygen simulations, *Global Biogeochem. Cycles*, 9, 621–636, 1995.
- Andres, R. J., D. J. Fielding, G. Marland, T. A. Boden, N. Kumar, and A. T. Kearney, Carbon dioxide emissions from fossil-fuel use, *Tellus, Ser. B*, 51, 759–765, 1999.
- Aumont, O., J. Orr, P. Monfray, G. Madec, and E. Maier-Reimer, Nutrient trapping in the equatorial Pacific: The ocean circulation solution, *Global Biogeochem. Cycles*, 13, 351–369, 1999.
- Aumont, O., S. Belviso, and P. Monfray, Dimethylsulfoniopropionate (DMSP) and dimethylsulfide (DMS) sea surface distributions simulated from a global three-dimensional ocean carbon cycle model, *J. Geophys. Res.*, 10, 1029/1999JC000111, in press, 2002.
- Barnett, T. P., D. W. Pierce, and R. Schnur, Detection of anthropogenic climate change in the world's oceans, *Science*, 292, 270–274, 2001.
- Battle, M., M. L. Bender, P. P. Tans, J. W. C. White, J. Ellis, T. Conway, and R. Francey, Global carbon sinks and their variability inferred from atmospheric O₂ and δ¹³C, *Science*, 287, 2467–2470, 2000.
- Beckmann, A., and R. Döschner, A method for improved representation of dense water spreading over topography in geopotential-coordinate models, *J. Phys. Oceanogr.*, 27, 581–591, 1997.
- Bender, M., T. Ellis, P. Tans, R. Francey, and D. Lowe, Variability in the O₂/N₂ ratio of Southern Hemisphere air, 1991–1994: Implications for the carbon cycle, *Global Biogeochem. Cycles*, 10, 9–21, 1996.
- Bindoff, N., and T. McDougall, Decadal changes along an Indian Ocean section at 32°S and their interpretation, *J. Phys. Oceanogr.*, 30, 1207–1222, 2000.

- Blanke, B., and P. Delecluse, Low frequency variability of the tropical Atlantic Ocean simulated by a general circulation model with mixed layer physics, *J. Phys. Oceanogr.*, **23**, 1363–1388, 1993.
- Bopp, L., P. Monfray, O. Aumont, J.-L. Dufresne, H. LeTreut, G. Madec, L. Terray, and J. Orr, Potential impact of climate change on marine export production, *Global Biogeochem. Cycles*, **15**, 81–99, 2001.
- Conkright, M. E., S. Levitus, and T. P. Boyer, *NOAA Atlas NESDIS 1: World Ocean Atlas 1994, vol. 1, Nutrients*, 150 pp., U.S. Dep. of Commer., Washington, D. C., 1994.
- Cox, P. M., R. A. Betts, C. D. Jones, S. A. Spall, and I. J. Totterdell, Acceleration of global warming due to carbon-cycle feedbacks in a coupled climate model, *Nature*, **408**, 184–187, 2000.
- Dufresne, J.-L., P. Friedlingstein, M. Berthelot, L. Bopp, P. Ciais, L. Fairhead, H. L. Treut, and P. Monfray, On the magnitude of positive feedback between future climate change and the carbon cycle, *Geophys. Res. Lett.*, in press, 2002.
- Emerson, S., S. Mecking, and J. Abell, The biological pump in the subtropical North Pacific Ocean: Nutrient sources, Redfield ratios, and recent changes, *Global Biogeochem. Cycles*, **15**, 535–554, 2001.
- Filiberti, M.-A., J.-L. Dufresne, and J.-Y. Grandpeix, Igloo sea-ice model version 1.0: Reference manual, notes techniques du pôle de modélisation, Inst. Pierre Simon LaPlace, Paris, 1999.
- Friedlingstein, P., I. Y. Fung, E. A. Holland, J. G. John, G. P. Brasseur, D. J. Erickson, and D. S. Schimel, On the contribution of the biospheric CO₂ fertilization to the missing sink, *Global Biogeochem. Cycles*, **9**, 541–556, 1995.
- Friedlingstein, P., L. Bopp, P. Ciais, J.-L. Dufresne, L. Fairhead, H. L. Treut, J. Orr, and P. Monfray, Positive feedback between future climate change and the carbon cycle, *Geophys. Res. Lett.*, **28**, 1543–1546, 2001.
- Gent, P. R., J. Willebrand, T. J. McDougall, and J. C. McWilliams, Parameterizing eddy-induced tracer transports in ocean circulation models, *J. Phys. Oceanogr.*, **25**, 463–474, 1995.
- Gibson, J. K., P. Killberg, S. Uppala, A. Hernandez, A. Nomura, and E. Serrano, ERA description, *ERA PRS 1*, 72 pp., Eur. Cent. for Medium-Range Weather Forecasts, Reading, England, 1997.
- Gruber, N., E. Gloor, S.-M. Fan, and J. L. Sarmiento, Air-sea flux of oxygen estimated from bulk data: Implications for the marine and atmospheric oxygen cycles, *Global Biogeochem. Cycles*, **15**, 783–803, 2001.
- Heimann, M., The global atmospheric tracer model TM2: Model description and user manual, *Tech. Rep. 10*, Max Planck Inst. für Meteorol., Hamburg, 1995.
- Houghton, J., et al. (Eds.), *Climate Change 2001: The Scientific Basis*, Cambridge Univ. Press, New York, 2001.
- Keeling, R. F., and S. R. Shertz, Seasonal and interannual variations in atmospheric oxygen and implications for the global carbon cycle, *Nature*, **358**, 723–727, 1992.
- Keeling, R. F., S. C. Piper, and M. Heimann, Global and hemispheric CO₂ sinks deduced from changes in atmospheric O₂ concentration, *Nature*, **381**, 218–221, 1996.
- Keeling, R. F., B. B. Stephens, R. G. Najjar, S. C. Doney, D. Archer, and M. Heimann, Seasonal variations in the O₂/N₂ ratio in relation to the kinetics of air-sea gas exchange, *Global Biogeochem. Cycles*, **12**, 141–164, 1998.
- Keeling, R. F., C. D. Keeling, and A. C. Manning, Atmospheric constraints on the uptake of carbon dioxide by the oceans and the land biota, *AMS Abstr. 5.8*, Am. Meteorol. Soc., Boston, Mass., 2001.
- Laurent, C., H. L. Treut, Z. X. Li, L. Fairhead, and J.-L. Dufresne, The influence of resolution in simulating inter-annual and inter-decadal variability in a coupled ocean-atmosphere GCM, with emphasis over the North Atlantic, *Notes Pole Model. IPSL 8*, Inst. Pierre Simon LaPlace, Paris, 1998.
- Lazar, A., G. Madec, and P. Delecluse, A rationalization of the Veronis upwelling/downwelling system and its sensitivity to mixing parameterizations in an idealized OGCM, *J. Phys. Oceanogr.*, **29**, 566–576, 1999.
- Le Quéré, C., J. C. Orr, P. Monfray, O. Aumont, and G. Madec, Interannual variability of the oceanic sink of CO₂ from 1979 through 1997, *Global Biogeochem. Cycles*, **14**, 1247–1265, 2000.
- Levitus, S., and T. P. Boyer, *NOAA Atlas NESDIS 2: World Ocean Atlas 1994, vol. 2, Oxygen*, U.S. Dep. of Commer., Washington, D. C., 1994.
- Levitus, S., J. I. Antonov, T. P. Boyer, and C. Stephens, Warming of the world ocean, *Science*, **287**, 2225–2229, 2000.
- Levitus, S., J. I. Antonov, J. Wang, T. L. Delworth, K. W. Dixon, and A. J. Broccoli, Anthropogenic warming of Earth's climate system, *Science*, **292**, 267–270, 2001.
- Liss, P., and L. Merlivat, Air-sea gas exchange: Introduction and synthesis, in *The Role of Air-Sea Exchange in Geochemical Cycling*, edited by P. Buat-Ménard, D. Reidel, Norwell, Mass., 1986.
- Machta, L., and E. Hughes, Atmospheric oxygen in 1967 to 1970, *Science*, **168**, 1582–1584, 1970.
- Madec, G., P. Delecluse, M. Imbard, and C. Lévy, OPA Version 8.0 ocean general circulation model: Reference manual, technical report, Lab. d'Océanogr. Dyn. et de Clim., Paris, 1997.
- Maier-Reimer, E., Geochemical cycles in an ocean general circulation model: Preindustrial tracer distributions, *Global Biogeochem. Cycles*, **7**, 645–677, 1993.
- Manabe, S., and R. J. Stouffer, Century-scale effects of increased atmospheric CO₂ on the ocean-atmosphere system, *Nature*, **364**, 215–218, 1993.
- Matear, R. J., A. C. Hirst, and B. I. McNeill, Changes in dissolved oxygen in the Southern Ocean with climate change, *Geochim. Geophys. Geosyst.*, **1**, 2000.
- McKinley, G. A., M. J. Follows, and J. Marshall, Interannual variability of the air-sea flux of oxygen in the North Atlantic, *Geophys. Res. Lett.*, **27**, 2933–2936, 2000.
- Najjar, R. G., and R. F. Keeling, Analysis of the mean annual cycle of the dissolved oxygen anomaly in the world ocean, *J. Mar. Res.*, **55**, 117–151, 1997.
- Najjar, R. G., and R. F. Keeling, Mean annual cycle of the air-sea oxygen flux: A global view, *Global Biogeochem. Cycles*, **14**, 573–584, 2000.
- Ono, T., T. Midorikawa, Y. W. Wanatabe, K. Tadokoro, and T. Saino, Temporal increase of phosphate and apparent oxygen utilization in the subsurface waters of western subarctic Pacific from 1968 to 1998, *Geophys. Res. Lett.*, **28**, 3285–3288, 2001.
- Orr, J., et al., Estimates of anthropogenic carbon uptake from four three-dimensional global ocean models, *Global Biogeochem. Cycles*, **15**, 43–59, 2001.
- Pahlow, M. U., and U. Riebesell, Temporal trends in deep ocean Redfield ratios, *Science*, **287**, 831–833, 2000.
- Plattner, G.-K., F. Joos, T. F. Stocker, and O. Marchal, Feedback mechanisms and sensitivities of ocean carbon uptake under global warming, *Tellus, Ser. B*, **53**, 564–592, 2001.
- Prentice, I. C., et al., The carbon cycle and atmospheric CO₂, in *Climate Change 2001: The Scientific Basis*, edited by J. T. Houghton et al., Cambridge Univ. Press, New York, 2001.
- Sadourny, R., and K. Laval, January and July performances of the LMD general circulation model, in *New Perspectives in Climate Modeling*, edited by Berger A., pp. 173–198, Elsevier, New York, 1984.
- Sarmiento, J. L., T. M. C. Hughes, R. J. Stouffer, and S. Manabe, Simulated response of the ocean carbon cycle to anthropogenic climate warming, *Nature*, **393**, 245–249, 1998.
- Severinghaus, J. P., Studies of the terrestrial O₂ and carbon cycles in sand dune gases and in Biosphere 2, Ph.D. thesis, Harvard Univ., Cambridge, Mass., 1995.
- Shaffer, G., O. Leth, O. Ulloa, J. Bendtsen, G. Daneri, V. Dellarossa, S. Hornmababal, and P.-I. Sehlstedt, Warming and circulation change in the eastern South Pacific Ocean, *Geophys. Res. Lett.*, **27**, 1247–1250, 2000.
- Smolarkiewicz, K. P., and T. L. Clark, The multidimensional positive definite advection transport algorithm: Further development and applications, *J. Comp. Phys.*, **67**, 396–438, 1986.
- Stephens, B. B., R. F. Keeling, M. Heimann, K. D. Six, R. Murnane, and K. Caldeira, Testing global ocean carbon cycle models using measurements of atmospheric O₂ and CO₂ concentration, *Global Biogeochem. Cycles*, **12**, 213–230, 1998.
- Suess, E., Particulate organic carbon flux in the ocean-surface productivity and oxygen utilization, *Nature*, **288**, 260–263, 1980.
- Terray, L., E. Sevault, E. Guilyardi, and O. Thual, The OASIS coupler user guide version 2.0, *Tech. Rep. TR/CMGC/95-46*, Eur. Cent. for Res. and Adv. Training in Sci. Comput., Toulouse, France, 1995.
- Tett, S., Simulation of El Niño—Southern Oscillation-like variability in a global AOGCM and its response to CO₂ increase, *J. Clim.*, **8**, 1473–1502, 1995.
- Weiss, R., The solubility of nitrogen, oxygen and argon in water and seawater, *Deep Sea Res.*, **17**, 721–735, 1970.
- White, W., and R. Peterson, An Antarctic circumpolar wave in surface pressure, wind, temperature and sea-ice extent, *Nature*, **380**, 699–702, 1996.

L. Bopp and P. Monfray, Institut Pierre-Simon Laplace/Laboratoire des Sciences du Climat et de l'Environnement, CE Saclay, L'Orme des Merisiers, F-91191 Gif sur Yvette Cedex, France. (bopp@lsce.saclay.cea.fr; monfray@lsce.saclay.cea.fr)

M. Heimann, C. Le Quéré, and A. C. Manning, Max-Planck Institut für Biogeochemie, Postfach 100164, D-07701 Jena, Germany. (heimann@atlas.bgc-jena.mpg.de; lequere@atlas.bgc-jena.mpg.de; amanning@atlas.bgc-jena.mpg.de)

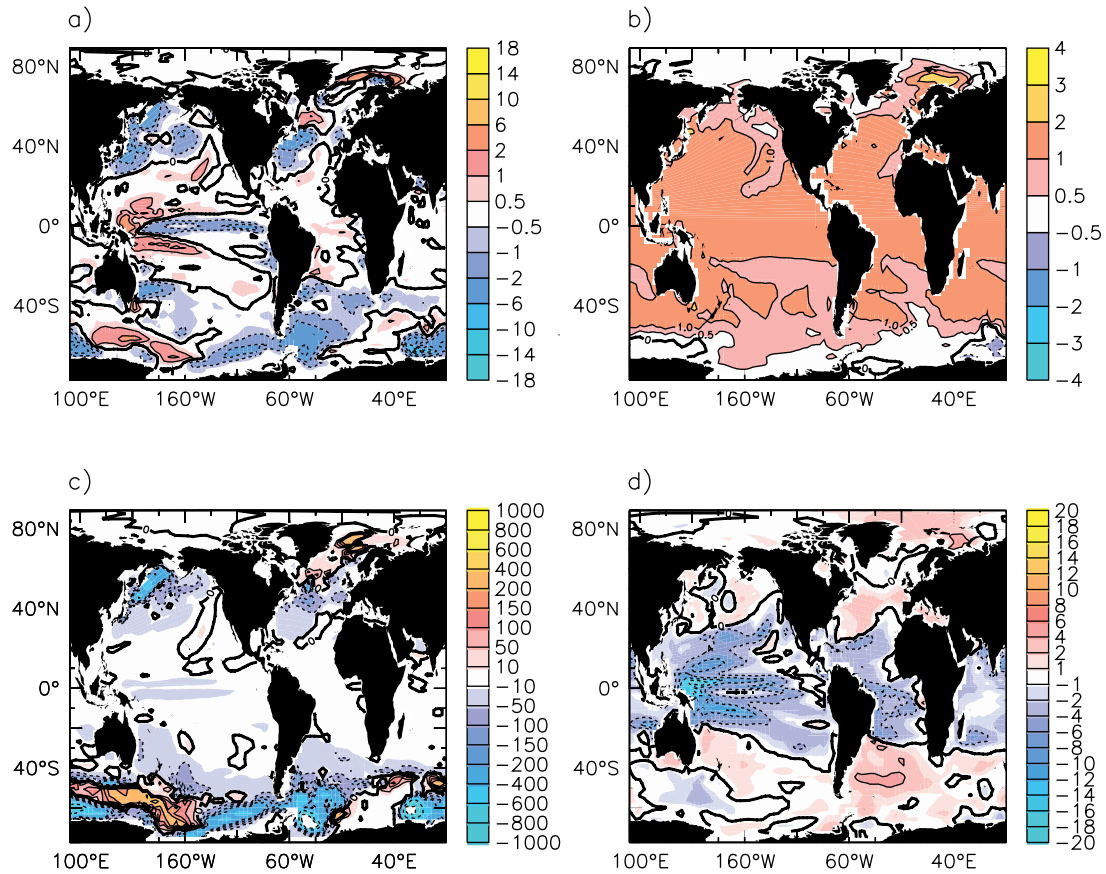


Figure 9. Climate change impact (difference between 2080–2100 and 1980–2000) on (a) O₂ fluxes (mol m⁻² yr⁻¹), (b) sea surface temperature (SST) (°C), (c) mixed layer depth (m), and (d) export production (g C m⁻² yr⁻¹).

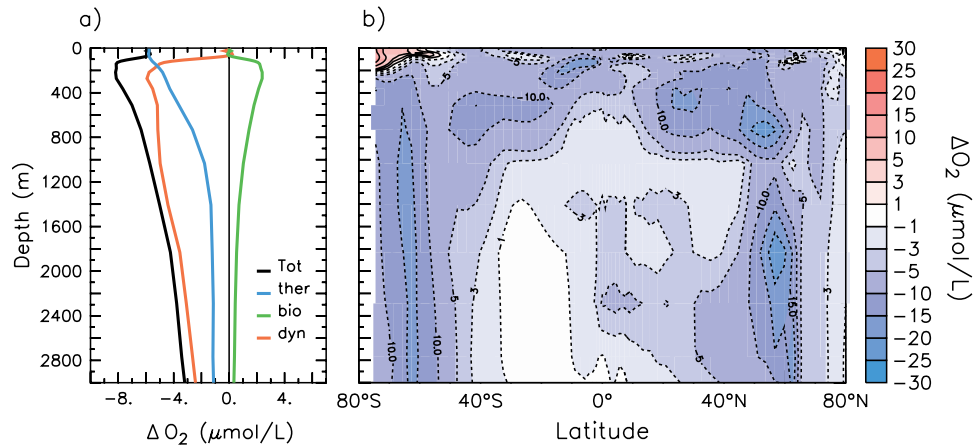


Figure 10. Climate change impact (difference between 2080–2100 and 1980–2000) on (a) vertical profile and (b) zonal mean of dissolved O₂ in the ocean (μmol L⁻¹). Contribution of thermal, production, and dynamical effects are also shown in Figure 10a. Thermal effect (blue) is from an additional biogeochemical simulation in which SSTs from the global warming climate run were used as the only impact of global warming on dissolved O₂. Production effect (green) was computed off line using regional changes of export production on O₂ local vertical profile. Dynamical effect (red) was deduced by subtraction from other effects.